I-V characteristics and the superconducting transition in polycrystalline $YBa_2Cu_3O_{7-\delta}$

W. M. Tiernan, R. Joshi, and R. B. Hallock
Laboratory for Low Temperature Physics, Department of Physics and Astronomy, University of Massachusetts, Amherst, Massachusetts 01003
(Received 14 December 1992)

We report experimental measurements of $\rho(T)$ and $\chi_{ac}(T)$ performed on four polycrystalline sintered $YBa_2Cu_3O_{7-\delta}$ samples that characterize the granular superconducting properties of these samples. We report I-V isotherm measurements near the superconducting transition at selected magnetic fields $0.5 \leq H \leq 80.9$ G for two of the samples. The observed I-V isotherms are consistent with recent predictions of superconducting I-V scaling, with critical exponents $\nu \approx 1.3-1.6$ and $z \approx 2.6-3.4$.

INTRODUCTION

In polycrystalline sintered pellets and epitaxial films, there have been several observations of a complex evolution of I-V characteristics near the superconducting transition. It is well established that superconductivity in sintered polycrystalline $YBa_2Cu_3O_{7-\delta}$ (YBCO) is determined by Josephson weak links at grain boundaries, and thus these materials provide an experimental realization of Josephson-array granular superconductivity. Dubson *et al.*[1] pointed out the two-stage nature of the superconducting transition and also the occurrence of power-law I-V characteristics near the $\rho \rightarrow 0$ transition. Power-law I-V characteristics have subsequently been observed in numerous studies.[2-5] Sergeenkov[6] has used a Josephson-array superconducting-glass model to predict I-V characteristics of the form $V \propto (I - I_c)^a$, in agreement with some of these experiments. More recently, I-V studies on sintered YBCO (Refs. 7–9) have found that I-V isotherms have a scaling form similar to that reported by Koch *et al.*[10] in epitaxial YBCO.

I-V and χ_{ac} measurements near T_c provide quite different and complementary information concerning the superconducting response of these materials and together help to provide a comprehensive understanding of the superconducting transition. A unique feature of this work is the collection of extensive sets of I-V and χ_{ac} measurements on single YBCO sintered pellets. Here, we report experimental measurements of $\rho(T)$ and $\chi_{ac}(T)$ near T_c for four sintered YBCO samples that characterize the nature of the granular superconducting transition. For two of these samples, we also report an extensive set of I-V isotherm measurements done at selected magnetic fields $0.5 \leq H \leq 81$ G that investigate possible critical behavior associated with the granular superconducting transition. Our I-V measurements were done at small current densities $10^{-3} \lesssim J \lesssim 10$ A/cm^2 with an electric field sensitivity of 2 nV/cm and a maximum range of six decades in voltage. A more extensive set of χ_{ac} measurements done on these samples is discussed separately in Ref. 11, and a more complete description of all of these measurements can be found in Ref. 12.

BACKGROUND

In this section we provide a brief overview of Josephson-array granular superconductivity and its applicability to sintered YBCO. We also discuss recent developments in the area of superconducting critical phenomena, in particular superconducting I-V scaling.

One consequence of the ceramic nature of YBCO is that any macroscopic three-dimensional sample consists of a large number of $\sim 1-10$ μm sintered YBCO grains which have a significant effect on the superconducting properties of the sample. Epitaxial YBCO, which has transport properties representative of single grain YBCO, typically has $J_c \approx 10^5$ A/cm^2 at 77 K and $\approx 10^6$ A/cm^2 at 4 K.[13] Bulk sintered polycrystalline YBCO on the other hand typically has $10^2 \lesssim J_c \lesssim 10^3$ A/cm^2 at 77 K and $J_c \sim 10^4$ at 4 K.[14,15]

A series of experiments performed by Dimos, Chaudhari, and Mannhart[16] on c-axis aligned polycrystalline YBCO films have convincingly demonstrated that Josephson weak links occur at YBCO grain boundaries, and have also shown that, for these c-axis aligned films, the weak-link behavior correlates with misalignment of the a and b crystal axes of adjacent grains. J_c values across misaligned boundaries are very sensitive to magnetic field. For $H < H_{c1}$, the field and temperature dependence of I-V characteristics were found to be typical of classical Josephson effect weak links. For $H > H_{c1}$, the I-V characteristics are more complex, but are still generally consistent with Josephson effect weak-link behavior.

As a result of weak links at grain boundaries, there are actually two distinct superconducting transitions in polycrystalline YBCO. The first occurs when individual grains become superconductors at a temperature T_{c0}. The second transition is associated with superconductivity of the sample as a whole and comes about because of Josephson currents between grains. An important parameter in determining the granular superconducting properties of polycrystalline YBCO is the relationship between the coherence length ξ and the YBCO grain sizes d_g. The single grain YBCO coherence length is $\xi_0 \sim 10$

0163-1829/93/48(5)/3423(10)/$06.00

Å, and grain sizes in a typical pellet range from 1 to 10 μm. Near T_{c0}, the single grain coherence length is expected to diverge as $\xi \sim \xi_0 |T - T_{c0}|^{-2/3}$.[17] From this, $\xi(T) \sim 0.1\,\mu\text{m} \lesssim d_g/10$ for $|T - T_{c0}| \approx 0.1$. Given that the $\rho \rightarrow 0$ transition in sintered YBCO occurs at least 1 K below T_{c0}, for polycrystalline sintered YBCO $\xi \ll d_g$.

The condition $\xi \ll d_g$ and the fact that integrain Josephson critical current densities are much less than intragrain critical current densities implies that each grain can be treated as an independent macroscopic superconductor with a well-defined superconducting order parameter $\psi = |\psi| e^{i\theta}$. As a result, polycrystalline YBCO should provide a good experimental realization of a Josephson-array granular superconductor. The following describes some of the work that has been done to understand these systems.

Deutscher, Imry, and Gunther[18] predicted that Josephson arrays could have an experimentally accessible critical region. Ebner and Stroud[19–21] and Shih, Ebner, and Stroud[22] investigated the magnetic-field-dependent behavior of three-dimensional disordered Josephson arrays based on Monte Carlo simulations. They pointed out that such systems provide an example of a gauge glass[21] and have many similarities to spin-glass systems. Spin glasses are dilute magnetic alloys in which competing ferromagnetic and antiferromagnetic interactions between spins frustrate the system's ability to form an ordered ground state.[23] John and Lubensky have investigated the behavior of disordered three-dimensional Josephson arrays using replica field theory methods.[24] More recently, Houghton and Moore[25] have used the techniques of Ref. 24 to show that in spite of the qualitative similarities between the two systems, disordered Josephson arrays should have different critical exponents than spin glasses. Until recently, there has been surprisingly little experimental work done on three-dimensional Josephson arrays. This is because, for metallic superconductors, it is difficult to achieve experimentally the conditions of relatively large grain size and small Josephson coupling required to produce a Josephson array. Before recent work on high-T_c superconductors, probably the most extensive experimental investigation on three-dimensional Josephson arrays was done by Rosenblatt.[26] Rosenblatt and co-workers performed a series of I-V and ac susceptibility measurements on fabricated three-dimensional (3D) Josephson arrays consisting of superconducting NbN spheres imbedded in epoxy. They interpreted their observations of power-law I-V characteristics[27] and bulk penetration depths near T_c (Ref. 28) in the context of XY model critical exponents. Recent work investigating the relationship between I-V characteristics and intergranular flux motion in ordered 2D arrays has been done by Benz and co-workers.[29,30] Recent I-V measurements on disordered 2D Josephson arrays have been done by Harris *et al.*, with results interpreted in the context of superconducting I-V scaling.[31]

The starting point for any Josephson-array model is the Josephson equations.[32] For a network of Josephson coupled grains, the Josephson current between adjacent grains i and j can be written as

$$I_{ij} = I_{ij}^0 \sin(\theta_i - \theta_j - A_{ij}) \ . \tag{1}$$

Here I_{ij}^0 is the Josephson critical current between grains i and j neglecting the effects of thermal fluctuations. I_{ij}^0 is not an experimentally accessible quantity. θ_i is the phase of the superconducting order parameter associated with grain i. The term A_{ij} depends on the vector potential $\mathbf{A}$ as

$$A_{ij} = (2\pi/\Phi_0) \int_i^j \mathbf{A} \cdot d\mathbf{r} \ , \tag{2}$$

where $\Phi_0 = hc/2e$ is the quantum of flux. Summing $A_{ij}/2\pi$ around a closed loop of grains gives the enclosed magnetic flux in units of the flux quantum Φ_0. The Josephson coupling energy between grains is

$$E_{ij}^J = -(\hbar/2e) I_{ij}^0 \cos(\theta_i - \theta_j - A_{ij}) \ . \tag{3}$$

The ability of the sample as a whole to sustain a zero-voltage current depends on the behavior of the θ_i degrees of freedom. Thermal fluctuations and current tend to cause the θ_i's to "slip," producing intergranular voltages $V_{ij} = d(\theta_i - \theta_j)/dt$. The I_{ij}^0 increase with decreasing temperature and, at some $T_c < T_{c0}$, the Josephson coupling energies may be strong enough to freeze the θ_i's, thus enabling a zero-voltage current to occur. If the magnetic field H is large enough, many of the $A_{ij} \sim \pi$, with the result that the A_{ij} become random, thereby destroying the ability of the θ_i's to have long-range order. In this case, the occurrence of bulk superconductivity is associated with a freezing of the θ_i's in some random configuration that results in a low system free energy. This state of frozen θ_i has been called a "gauge glass."[22,25] The gauge glass condition, $A_{ij} \sim \pi$, occurs when there is $\approx \Phi_0/2$ per typical grain cross section, and this condition defines a characteristic gauge glass magnetic field H_g as

$$H_g = \Phi_0 / 2 l_g^2 \ . \tag{4}$$

Here l_g is a length scale that characterizes the granularity of the sample, and should be comparable to the average grain size $\langle d_g \rangle$. For a typical YBCO sintered pellet, $\langle d_g \rangle \sim 5\ \mu$m, so that $H_g \sim 0.4$ G.

Superconductivity in polycrystalline YBCO is governed by the behavior of the superconducting phases θ_i and in the critical region superconducting properties presumably result from critical fluctuations in the θ_i. The A_{ij} terms in Eq. (3) have a significant impact: if these terms are non-negligible, then the system is a gauge glass and there is no ordered ground state of the θ_i. The lack of long-range order in the θ_i should not preclude the possibility of a zero-voltage current as long as the θ_i are frozen; however, the differences in ground-state ordering may be significant to critical behavior. The behavior of critical fluctuations near T_c depends on the interactions between adjoining regions with different order parameters. The surface energies associated with domain walls between these regions will be very different for gauge glass phases than for conventionally ordered phases. For a conventional ordering transition in three-dimensional systems, $\nu \approx 0.5$–0.7 and $z \approx 2$.[33] In three-dimensional spin glasses, on the other hand, these exponents have somewhat higher values, $\nu \approx 1.3$ and $z \approx 4$–7.[23]

There has been recent work done concerning supercon-

ductivity in type-II superconductors that directly considers questions of ordering and critical behavior in glasslike systems. Fisher[34] has proposed that the flux lattice in a type-II superconductor freezes into a glasslike order, a "vortex glass," at a glass temperature T_g. A vortex glass lacks long-range order, but flux vortices are frozen and thus can support zero-voltage currents. A connection between vortex glass systems and gauge glasses can be made by comparing dissipative mechanisms in the two systems. Although there is no well-defined flux lattice in a gauge glass, a transport current causes slippage in the θ_i that results in dissipation. Below T_c, where the θ_i are coupled, the collective modes of phase slippage should be expressible in terms of flux motion across the sample, which is directly analogous to the situation in vortex glasses. The connection between phase slip and vortex motion has been used successfully to describe the behavior of two-dimensional Josephson arrays.[29,30] Although a connection between the methods of dissipation for these two systems can be made, the types of energy barriers that flux vortices are affected by in the two systems are probably very different. For ordered two-dimensional Josephson arrays, the energy barriers are related to the Josephson coupling energy.[29,30]

I-V isotherm measurements performed by Koch *et al.*[10] on epitaxial YBCO at $0.5 \leq H \leq 4$ T were found to have a scaling form analogous to $M(H)$ scaling seen in ferromagnetic systems. Motivated by these results as well as by earlier I-V measurements done on superconducting films,[35,36] Fisher, Fisher, and Huse[17] (FFH) have proposed an I-V scaling hypothesis. The FFH scaling hypothesis predicts an explicit form for the evolution of I-V isotherms that allows for the extraction of critical exponents from I-V isotherm measurements. FFH propose that I-V isotherms near T_c have the following form:

$$E \sim J\xi^{d-2-z}\tilde{\mathcal{E}}_{\pm}(J/J_0) . \tag{5}$$

Here ξ is the coherence length, d is the dimensionality of the system, and z is the dynamical critical exponent.[33,37] $\tilde{\mathcal{E}}_{\pm}(x)$ are scaling functions above $(+)$ and below $(-)$ T_c. J_0 is a characteristic current roughly equivalent to J_c, and is predicted to depend on ξ as $J_0 \sim \xi^{-(d-1)}$. If ξ diverges near T_c as $\xi \sim |\vartheta|^{-\nu}$, consistent with scaling hypotheses, then Eq. (5) can be written in terms of reduced temperature,

$$E \sim J|\vartheta|^{\mu}\tilde{\mathcal{E}}_{\pm}(J/|\vartheta|^{\lambda}) . \tag{6}$$

This form is useful since ϑ, μ, and λ are quantities that can be experimentally determined from I-V isotherm measurements. In Eq. (6), $\mu = \nu(z+2-d)$ and $\lambda = \nu(d-1)$.

The I-V isotherms measured by Koch *et al.*[10] were consistent with the FFH scaling hypothesis, and their extracted critical exponents of $\nu \approx 1.5$ and $z \approx 4.5$ were interpreted as evidence for a vortex glass transition. There have also been experimental observations of I-V scaling in sintered YBCO. Worthington *et al.*[8] have measured I-V isotherms in bulk sintered YBCO at magnetic fields of $0.5\times10^3 \leq H \leq 4\times10^3$ G and obtained results consistent with the FFH scaling hypothesis. They extracted critical exponents $\nu \approx 1.1 \pm 0.2$ and $z \approx 4.6 \pm 0.2$. These exponents are similar to those found by Koch *et al.* for epitaxial YBCO, and suggest that vortex glass and gauge glass systems may have similar critical exponents. More recently, based on some of the results described in this work, Tiernan and Hallock[9] have reported I-V scaling in sintered YBCO for $0.5 \leq H \leq 80.9$ G consistent with $\nu \approx 1.4$ and $z \approx 3.0$.

APPARATUS AND EXPERIMENTAL TECHNIQUES

A closed-cycle refrigeration system[38] was used for the I-V isotherm measurements. The sample block is separated from the low-temperature (LT) stage of the cold head by a 13×250 mm^2 Cu connecting rod (Fig. 1) in order that samples could be positioned between the pole pieces of an electromagnet. The sample platform and a platinum thermometer are covered by a copper radiation shield that is anchored to the sample block. The sample-block–connecting-rod assembly is enclosed by an aluminum radiation shield screwed onto the 77-K stage of the cold head. The entire assembly is enclosed in a vacuum jacket. Electrical leads are heat sunk at the LT stage and at the sample block. A more complete description of the refrigeration system can be found in Ref. 12.

Temperature regulation was accomplished using a Lakeshore model LS805 temperature controller, which monitored the temperature of a Lakeshore DT 470 diode thermometer attached to the LT stage and controlled power output to a 25-Ω manganin wire bifilar heater attached to the LT stage with GE 7031 varnish. The temperature of the sample block was measured with a Lakeshore PT-111 platinum thermometer. Sample block temperature was monitored during I-V isotherm mea-

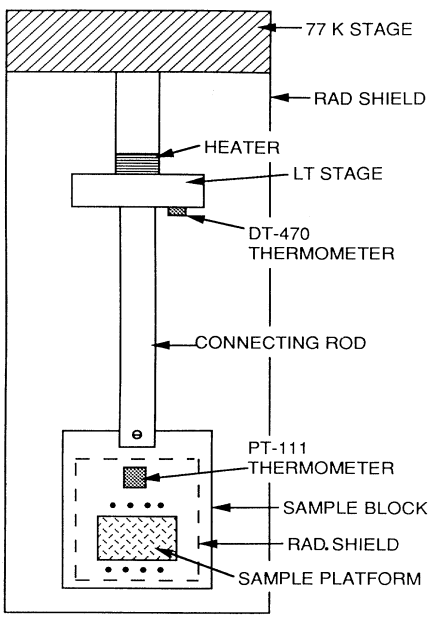

FIG. 1. Schematic of the sample block, connecting rod assembly, and refrigeration stages.

surements and observed to be constant with a rms deviation $\delta T \approx 1-2$ mK. The heat load on the sample stage due to Joule heating during I-V measurements was small and caused negligible temperature changes on the sample block.

Our I-V measurements were done at small current densities $10^{-3} \lesssim J \lesssim 10$ A/cm^2 with an electric field sensitivity of 2 nV/cm and a maximum range of six decades in voltage. These values are comparable to those obtained by Worthington *et al.*,[8] and were chosen to be sensitive to possible I-V critical behavior at low current densities. Our I-V isotherm measurements are reported in the sample-independent units of electric field E versus current density J. For a sample with constant cross-sectional area A, uniform current density J, and a length l between voltage contacts, $E = V/l$ and $J = I/A$; V and I were the directly measured quantities.

A schematic of the circuit used for dc I-V measurements is shown in Fig. 2. dc voltages were measured by HP 3478A multimeters using the standard four-lead technique to a sensitivity limit of $\delta V \approx 0.1$ μV. Sample current was determined by measuring the voltage across a calibrated wirewound resistor ($R = 0.9988\Omega$) in series with the sample. For each single I-V measurement, the current was reversed in order to eliminate thermal voltages. For $R(T)$ runs, temperature was monitored and data taking was controlled by computer through a GPIB bus to the voltmeters.

Greater voltage sensitivity can be achieved using phase-sensitive ac techniques. In this approach the sample current is a low-frequency square wave and the resulting sample voltage is measured with a lock-in amplifier. The frequency of the square wave is chosen to be low enough so that the measured voltage results from the dc response of the sample during the constant current cycle of the square wave driving current. Our apparatus had a voltage sensitivity $\delta V \approx 1$ nV. Figure 3 shows a schematic of the circuit used for ac I-V measurements. The sample current was a 10.5-Hz square wave.

Sample voltages were measured using the standard four-lead technique, employing separate contacts for current and voltage leads. Two methods were used to make electrical contact to the samples. For current contacts, low resistance contacts were obtained using a technique similar to that described by Ekin and coworkers.[39,40] Ag pads $\approx 2\,\mu$m thick were evaporated near the ends of the sample, and the sample was annealed in flowing O_2 at $T = 550\,^\circ$C for 1 h. Current leads were then attached to these annealed Ag pads with In solder. The contact resistance of one such current contact was measured using a four-lead technique and found to be < 0.2 mΩ. With annealed Ag contacts, Joule heating at the current contacts was found to cause negligible temperature changes for sample currents up to 200 mA. Voltage contacts were made using Ag filled paint, which resulted in a typical contact resistance of $\sim 1\Omega$ and fair mechanical strength.

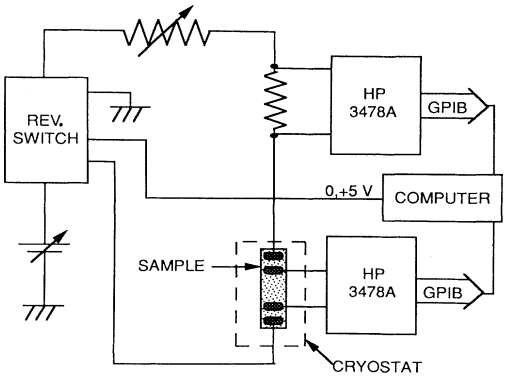

FIG. 2. Schematic of circuit used for dc I-V measurements.

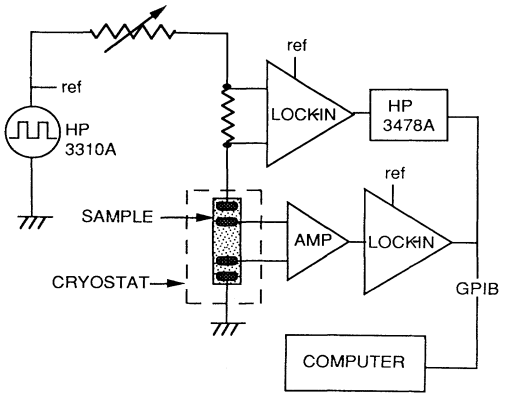

FIG. 3. Schematic of circuit used for ac I-V measurements.

Some of the I-V runs were done in the local ambient magnetic field B_e. B_e was measured to have a magnitude $B_e = 0.5$ G and forms an $\approx 15°$ angle with respect to local vertical. In addition, a 12-in. electromagnet with a modified power supply was employed and could provide fields $0.1 \leq H \leq 10^4$ G. Magnetic field was measured using a Hall effect gaussmeter, with a range of 0.1 to 10^4 G. Measurements of H with the Hall probe showed that the vertical component between the pole pieces was less than 0.1 G. For the I-V measurements reported here, H was applied horizontally and perpendicular to the sample axis; the sample axis is the direction of the transport current. All measurements were performed after the sample was cooled into the superconducting state in the presence of the applied field H.

MATERIALS SYNTHESIS AND CHARACTERIZATION

Our samples are pressed and sintered pellets made from YBCO powder fabricated using the polymer-metal-complex technique,[4,41,42] which is an alternative to standard solid-state techniques of producing sintered ceramic superconductors. We have produced superconducting YBCO sintered pellets by this technique using calcination and sintering temperatures ranging from 880 to 950 °C.[4,12] Typically, samples with the best superconducting properties were fabricated at processing temperatures $920 \lesssim T \lesssim 940\,^\circ$C. At these temperatures we were able to produce sintered pellets with reproducible properties of density ≈ 5.2 g/cm^3, $\rho(300\text{ K}) \approx 1.1$ mΩ cm, and narrow

(≈ 1 K) superconducting transition regions. A density of 5.2 g/cm^3 is 84% of the YBCO single-crystal density of 6.2 g/cm^3. Processing conditions and characteristics of the four samples discussed in this work are listed in Table I. The values of density and ρ listed in Table I are limited to an accuracy of about 5% due to irregularities in sample dimensions.

Since grain boundaries play a key role in determining the superconducting behavior of sintered YBCO, it is useful to know the distribution of grain sizes and shapes. Following the measurements, the samples were fractured, and several scanning electron microscopy (SEM) images were taken at representative points of the cross section. A subset of $N_t \sim 200$ grains was selected from the SEM images by drawing a series of roughly parallel lines through the photographs. The linear dimensions of N_t grains that intersected the lines was measured and the grain size d_g was taken to be the geometric mean ($\sqrt{xy}$) of the two dimensions. The grain size distribution of the selected grains was determined by counting the number of grains $N(d_g)$ with d_g falling within a 1-μm interval centered on integer μm grain sizes. The frequency distribution $F(d_g)$ was estimated by $F(d_g)=N(d_g)/N_t$, and is shown in Fig. 4 for sample 331. $F(d_g)$ is sharply peaked around $d_g \approx 3$ μm. For 8 μm $\lesssim d_g \lesssim 12$ μm there were a relatively small number of grains, $0 \leq N(d_g) \leq 6$, and for this small sample of grains $F(d_g)$ appears to be more or less independent of d_g. In the set of selected grains, there was only one grain with $d_g > 12$ μm, and it had $d_g = 15$ μm.

For most of the samples, the largest number of grains were found to have sizes $d_g \leq 5$ μm; however, these small grains may occupy a relatively small volume and thus may not be significant in determining bulk superconducting properties of the sample. In order to estimate the relative volume occupied by a given grain size, we estimated the volume fraction as $F(V_g)=(d_g/\langle d_g \rangle)^3 F(d_g)$. $\langle d_g \rangle$ is an average grain size, and was taken to be the d_g coinciding with the peak in $F(V_g)$. $F(V_g)$ is shown in Fig. 4 for sample 331. $F(V_g)$ is a much broader distribution than $F(d_g)$ and has a peak at $d_g \approx 5$ μm. Because of the relatively small number of grains counted for $d_g \gtrsim 6$ μm there is a lot of scatter in $F(V_g)$ in this range. However, even if $F(V_g)$ goes smoothly to zero at $d_g \approx 12$ μm, grains with $d_g > 6$ μm appear to occupy a relative volume

TABLE I. Selected properties of the YBCO sintered pellets discussed in the text. All of the samples were sintered at 940 °C. Superconducting transition temperatures are for magnetic field $H = 0.5$ G.

	Sample no.			
	331	1765	1762	1333
Sinter time (h)	10	2	2	10
Density (g/cm^3)	5.4	5.1	5.0	5.4
ρ(300 K) (mΩ cm)	1.2	1.0	1.1	1.2
T_{c0} (K)	91.83	91.65	91.79	92.42
T_c (K)	90.83		90.50	
$\langle d_g \rangle$ (μm)	5	6	6	12
δd_g (μm)	6	5	4	6

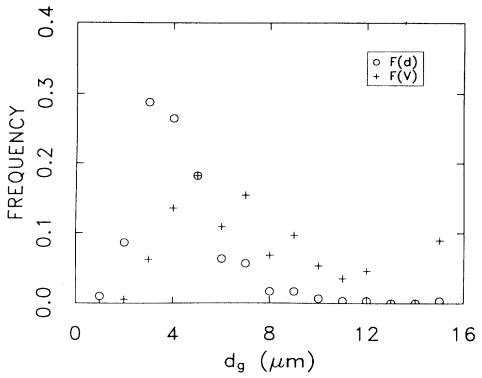

FIG. 4. Grain size distribution for sample 331.

greater than the percolation threshold. The volume percolation threshold in 3D is $\phi_c \approx 0.16$.[43] Based on $F(V_g)$, it is reasonable to expect that the transport properties of sample 331 should be determined primarily by grains with 4 μm $\lesssim d_g \lesssim 10$ μm. Grain size information for the four samples is summarized in Table I. In addition to $\langle d_g \rangle$, for each sample the width of the grain size distribution, δd_g, was estimated from the full width at half maximum of $F(V_g)$.

X-ray diffractograms of these samples were taken, and the results for samples 331 and 1765 are shown in Fig. 5. These are consistent with results expected for $YBa_2Cu_3O_{7-\delta}$.

EXPERIMENTAL RESULTS AND DISCUSSION

Figure 6 shows ρ vs T and χ_{ac} vs T near the superconducting transition for the four samples described in Table I. The features of ρ and χ_{ac} in all of these samples are consistent with a two-stage superconducting transition, with individual grains having a superconducting transition at T_{c0} and the sample as a whole having a granular

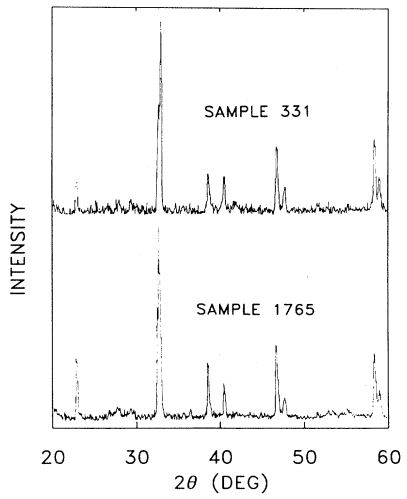

FIG. 5. X-ray diffractograms for samples 331 and 1765.

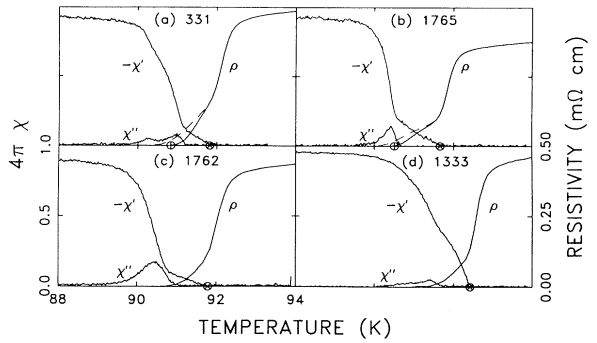

FIG. 6. $\rho(T)$ and $\chi_{ac}(T)$ near the superconducting transition at $H=0.5$ G. (a) Sample 331. (b) Sample 1765. (c) Sample 1762. (d) Sample 1333. ⊗ marks T_{c0} and ⊕ marks T_c. In (a) and (b), the dashed line shows the effect of an $H=8$ G magnetic field on $\rho(T)$.

superconducting transition at a lower temperature T_c. The structure of $\rho(T)$ at $H=0$ is very similar in all four samples shown in Fig. 6. The relatively abrupt drop in ρ above T_{c0} is attributable to fluctuation conductivity occurring in individual grains.[41,44–46] Below T_{c0}, ρ drops more gradually and has a footlike structure. This resistive "foot" is attributable to resistance at grain boundaries that result from the relatively weak Josephson coupling just below T_{c0}. In Figs. 6(a) and 6(b), the dashed line shows the effect of an $H=8$ G magnetic field on $\rho(T)$. The broadening of the resistive foot in this relatively small field is symptomatic of the Josephson coupling between YBCO grains. The insensitivity of $\rho(T)$ to the 8-G field for $T\gtrsim 92$ K suggests that for these temperatures $\rho(T)$ reflects intrinsic superconducting properties of the YBCO grains themselves.

χ' is the component of χ_{ac} in phase with the sinusoidal excitation field H_{ac} and χ'' is the component of χ_{ac} out of phase with H_{ac}. For $92\gtrsim T\gtrsim 91.5$ K, $-\chi'$ increases roughly linearly with decreasing temperature, and $\chi''=0$. This type of behavior is consistent with a diamagnetic response due to the Meissner effect in a collection of small, uncoupled superconducting particles with size $d_g \ll \lambda$. Here λ is the superconducting penetration depth. In such a system the $\chi'=0$ intercept gives the transition temperature of the grains, T_{c0}. T_{c0} determined in this way agrees with the onset of the intergranular "foot" region as deduced from $\rho(T)$ in Figs. 6(a)–6(d). χ' has a somewhat different structure for sample 1333 [Fig. 6(d)] compared with the other three samples. This may be attributable to the significantly larger grain sizes in sample 1333. From Table I, sample 1333 has an average grain size of 12 μm, twice that of the other three samples and also has a significantly larger value for T_{c0}.

I-V measurements performed on samples 331 and 1765 that are discussed later provide a determination of the granular superconducting transition temperature of the entire sample, T_c. The T_c determined from I-V characteristics occurs near the temperature for which ρ appears to go to zero in Figs. 6(a) and 6(b). The granular superconducting transition depends on the relationship between the intergranular Josephson coupling energy, $(\hbar/2e)I_{ij}^0$, and the thermal energy k_BT. Just below T_{c0}, the grains are superconducting but the intergranular Josephson coupling is small compared to k_BT. In this weak Josephson coupling regime, the YBCO grains are independent uncoupled superconductors and the grain boundaries are resistive. Further below T_{c0}, however, intergranular Josephson coupling becomes stronger and as a result ρ drops and appreciable intergranular Josephson currents develop. The effects of stronger Josephson coupling are manifested in the development of changes in both χ_{ac} and I-V characteristics. χ_{ac} develops a significant out-of-phase component χ'', and both χ' and χ'' become sensitive to changes in H_{ac}. These complex H_{ac} dependent changes in χ_{ac} are discussed in detail in Ref. 11. I-V measurements show that these changes in χ_{ac} are accompanied by the development of complex nonlinear I-V characteristics, as we next discuss.

I-V isotherm measurements were performed on sample 331 at $H=0.5$, 8.1, and 80.9 G and on sample 1765 at $H=0.5$ G. For each set of measurements, the I-V characteristics became nonlinear below T_{c0} and the structure of the I-V isotherms evolved in a distinctive way. Figure 7 shows selected I-V isotherms near the $\rho\rightarrow 0$ transition for sample 331 at $H=0.5$, 8.1, and 80.9 G and for sample 1765 at $H=0.5$ G. For both samples, $l\approx 0.65$ cm and $A\approx 0.023$ cm^2. The I-V isotherms all show a similar evolution in structure. They are entirely Ohmic near T_{c0}, and with decreasing temperature remain Ohmic at low currents, but become nonlinear at higher currents. The region of Ohmic behavior is reduced to smaller currents with decreasing temperature, until at some temperature there is no trace of Ohmic behavior and the I-V isotherms obey a power law, $V\propto I^a$, for more than three decades in voltage. At lower temperatures, the I-V isotherms exhibit a superconducting character, as evidenced by the negative curvature of $d\log V/d\log I$ over the entire range of experimental accessibility.

Similar evolution in I-V isotherms has been seen in a variety of superconducting systems, and is believed to be a characteristic feature of superconducting phase transitions. In the following we interpret the I-V isotherms of Fig. 7 in the context of the I-V scaling hypothesis proposed by Fisher, Fisher, and Huse[17] described earlier. The critical temperature T_c is associated with the occurrence of power-law I-V behavior, $V\propto I^a$. Based on our measurements, we could not determine a single temperature at which power-law behavior occurred, rather there was a range $\delta T\sim 20$–100 mK wide, depending on the sample and H, over which the I-V data were consistent with power-law behavior. At each field we estimated the center and width of the region of power-law behavior, and determined the power-law exponent a from the slope of $\log V$ vs $\log I$. Table II lists these results for both samples at $H=0.5$ G along with a number of other measurements that will be discussed later in this section. Table III lists these measurements for sample 331 at $H=0.5$, 8.1, and 80.9 G. The uncertainties in T_c and a given in Tables II and III represent the range of values consistent with the range δT of power-law I-V behavior.

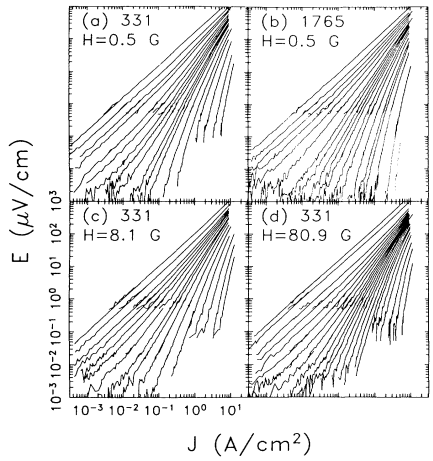

FIG. 7. I-V isotherms for samples 331 and 1765. (a) Sample 331, $H=0.5$ G. The temperature of each isotherm, from upper left to lower right, is $T=91.78$, 91.478, 91.338, 91.225, 91.134, 91.067, 91.006, 90.966, 90.916, 90.849, 90.812, 90.772, 90.678, 90.571, 90.471, 90.299, 90.073, and 89.866 K. (b) Sample 1765, $H=0.5$ G. $T=91.459$, 91.053, 90.908, 90.806, 90.724, 90.645, 90.559, 90.522, 90.484, 90.45, 90.42, 90.366, 90.312, 90.221, 90.134, 90.087, 89.975, 89.745, and 89.567 K. (c) Sample 331, $H=8.1$ G. $T=91.502$, 91.179, 90.944, 90.848, 90.737, 90.651, 90.542, 90.415, 90.346, 90.225, 90.053, 89.831, 89.588, 89.256, 88.855, and 88.522 K. (d) Sample 331, $H=80.9$ G. $T=91.743$, 91.236, 90.033, 89.523, 89.191, 88.938, 88.714, 88.512, 88.306, 88.156, 88.003, 87.85, 87.661, 87.477, 87.24, 86.965, 86.633, 86.361, 85.852, 85.241, 84.253, 83.261, and 81.902 K.

Superconducting I-V scaling should occur at current densities $J<k_BT/\Phi_0 l_J^2$, where l_J is a cutoff length scale above which the sample appears homogeneous.[8,17] For a polycrystalline sintered sample l_J should be related to the length scale associated with the granularity of the sample, $l_J\sim\langle d_g\rangle$. In Fig. 7, deviations from power-law behavior occur for $J\gtrsim 1$ A/cm^2. This is consistent with a length scale $l_J\sim 10$ μm, which is in accord with the average grain size $\langle d_g\rangle\approx 6$ μm.

Above T_c and for low currents, the I-V isotherms show Ohmic behavior consistent with a sample resistivity ρ_L. ρ_L was determined for several temperatures above T_c for sample 331 at $H=0.5$, 8.1, and 80.9 G and for sample 1765 at $H=0.5$ G. Figure 8 shows I-V data at selected temperature values and ρ_L fits for sample 331 done at $H=0.5$ G. For the three sets of data closest to T_c and having the lowest ρ_L values, each voltage represents an average of five independent measurements and the symbol-sized error bars give a 1σ statistical uncertainty. Plots of ρ_L vs T determined from extensive data similar to that shown in Fig. 8 for sample 331 at $H=0.5$, 8.1, and 80.9 G are shown in Fig. 9. Figure 10 shows ρ_L vs T for samples 331 and 1765 at $H=0.5$ G. It is clear from Figs. 9 and 10 that ρ_L drops very sharply as $T\rightarrow T_c$.

Figure 11(a) shows the ρ_L data of Fig. 9 plotted versus reduced temperature, $\vartheta=(T-T_c)/T_c$. Here T_c is determined from the occurrence of power-law I-V isotherms and is given in Table III. Figure 11(a) illustrates that for each value of the magnetic field, ρ_L near T_c is consistent with a power law of the form $\rho_L\sim\vartheta^{\mu}$, with μ apparently independent of H. Based on the previously described uncertainties in T_c, the power-law fits are consistent with $\mu=3.2\pm0.4$, 3.4 ± 0.6, and 3.3 ± 0.4 for $H=0.5$, 8.1, and 80.9 G, respectively. Figure 11(b) shows ρ_L vs ϑ for sample 1765 at $H=0.5$ G; here $\mu=2.8\pm0.6$, and T_c is that listed in Table II.

The agreement of our data with the FFH scaling form, Eq. (6), can be checked globally by performing a "data collapse." A data collapse consists of plotting $E/J|\vartheta|^{\mu}$ vs $J/|\vartheta|^{\lambda}$. If the data are consistent with the scaling form predicted by Eq. (6), then I-V data plotted in this way will lie on the two scaling curves $\tilde{\mathcal{E}}_{\pm}(J/|\vartheta|^{\lambda})$. Data collapses were done using T_c determined by the occurrence

TABLE II. Summary of critical temperatures and measured power-law exponents for samples 331 and 1765 at $H=0.5$ G. μ and λ were determined from data collapses.

	Sample no. 331	1765
T_{c0} (K)	91.83	91.65
T_c (K)	90.83±0.03	90.50±0.02
a	2.13±0.1	1.95±0.1
μ	3.1±0.2	2.8±0.2
λ	2.8±0.2	3.0±0.2
ν	1.4±0.1	1.5±0.1
z	3.2±0.2	2.8±0.2

TABLE III. Summary of critical temperatures and measured power-law exponents for sample 331 at $H=0.5$, 8.1, and 80.9 G. μ and λ were determined from data collapses.

H (G)	0.5	8.1	80.9
T_{c0} (K)	91.83	91.78	91.71
T_c (K)	90.83±0.03	90.23±0.1	87.95±0.1
a	2.13±0.1	2.15±0.15	2.15±0.1
μ	3.1±0.2	3.1±0.2	3.1±0.2
λ	2.8±0.2	2.8±0.2	2.8±0.2

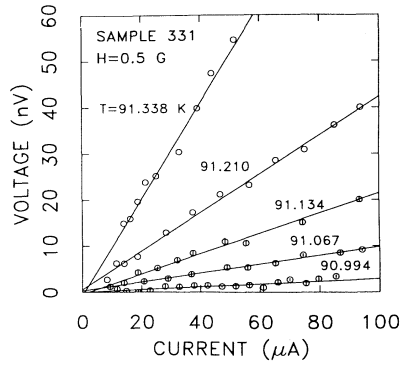

FIG. 8. Selected I-V data and ρ_L fits for sample 331 at $H=0.5$ G.

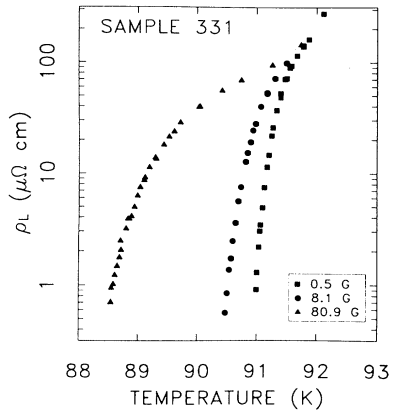

FIG. 9. ρ_L vs T for sample 331 at $H=0.5$, 8.1, and 80.9 G.

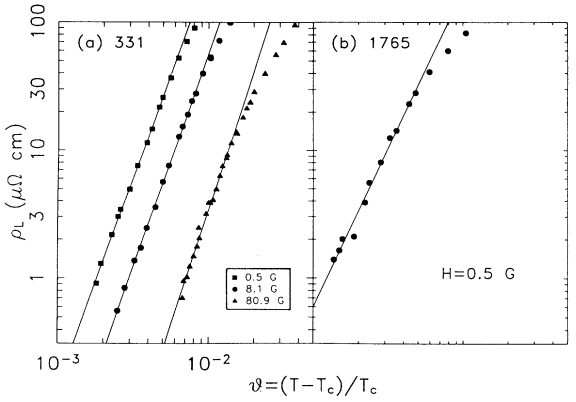

FIG. 11. ρ_L vs reduced temperature ϑ. (a) Sample 331 at $H=0.5$, 8.1, and 80.9 G. (b) Samples 331 and 1765 at $H=0.5$ G.

of power-law I-V characteristics and various combinations of μ and λ. Figures 12(a), 12(c), and 12(d) show data collapses for samples 331 at $H=0.5$, 8.1, and 80.9 G using $\mu=3.1$ and $\lambda=2.8$. At each field, these values of μ and λ caused the I-V isotherms to lie on the two scaling functions $\tilde{\mathcal{E}}_{\pm}(x)$, with the exceptions of expected deviations for large values of J and ϑ. A change of either μ or λ of ± 0.3 from these values produced significant and systematic deviations from the two scaling functions. Figure 12(b) shows a data collapse for sample 1765 at $H=0.5$ G. The optimum data collapse for sample 1765 was obtained using $\mu=2.8$ and $\lambda=3.0$.

The data collapses for each of Figs. 12(a)–12(d) primarily lie on two curves, and the shapes of the curves are consistent with the expected shapes of the scaling functions $\tilde{\mathcal{E}}_{\pm}(x)$. In particular, the data collapse for sample 331 at all fields is very good, with the only significant deviations from the scaling curves occurring for large values of J and ϑ, where deviations are expected. There are systematic deviations from the scaling curves in sample 1765. Based on SEM photos[12] sample 1765 appears to have some relatively large-scale holes and cracks, and these may have an effect on scaling behavior. χ_{ac} measurements discussed in Ref. 11 are also consistent with sample 1765 having a larger degree of inhomogeneity than sample 331.

For sample 331, acceptable data collapses with various values of T_c, μ, and λ provided the following limits on μ and λ: $\mu=3.1\pm0.2$ and $\lambda=2.8\pm0.2$. For sample 1765, $\mu=2.8\pm0.2$ and $\lambda=3.0\pm0.2$. I-V scaling, Eq. (6), provides the relationship $a=1+\mu/\lambda$, which agrees very well with our measurements. For sample 331, $a\approx 2.13\pm0.1$, whereas $1+\mu/\lambda\approx 2.11\pm0.1$. For sample 1765, $a=1.95\pm0.1$, whereas $1+\mu/\lambda=1.93\pm0.1$.

The I-V scaling equations, (5) and (6), provide relationships between the experimentally measurable exponents a, μ, and λ and the more fundamental critical exponents ν and z. ν is the coherence length critical exponent, and gives the dependence of coherence length ξ on ϑ, $\xi\sim\vartheta^{-\nu}$. z is the dynamical critical exponent, and gives the diver-

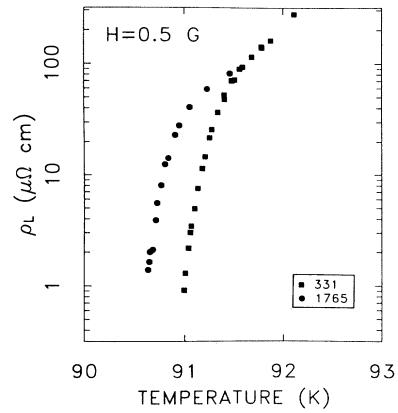

FIG. 10. ρ_L vs T for samples 331 and 1765 at $H=0.5$ G.

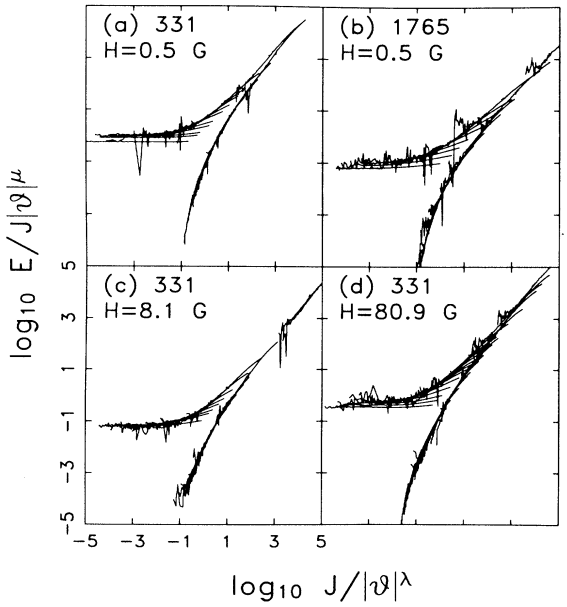

FIG. 12. Data collapses for the I-V isotherm data of Fig. 7.

gence of characteristic relaxation times τ near T_c, $\tau \sim \xi^z$. Equations (5) and (6) give, for $d=3$, $z=2a-1$, $\nu=\lambda/2$, and $\nu=\mu/(z-1)$. For sample 331, the measured values of $a=2.13\pm0.1$, $\lambda=2.8\pm0.2$, and $\mu=3.1\pm0.2$ yield $z=3.26\pm0.2$, $\nu=1.4\pm0.1$, and $\nu=1.37\pm0.1$. For sample 1765, $a=1.95\pm0.1$, $\lambda=3.0\pm0.2$, and $\mu=2.8\pm0.2$ give $z=2.8\pm0.2$, $\nu=1.5\pm0.1$, and $\nu=1.56\pm0.1$. Thus the critical exponents that we obtain are consistent with predictions of Eqs. (5) and (6).

Our results for ν and z can be compared with theoretical predictions and with measurements on other superconducting systems. ν has been calculated using first-order ϵ expansions for several different systems. For the XY model, $\nu \approx 0.67$.[33] For a spin glass with a two-component order parameter, $\nu \approx 1.33$, whereas for a two-component gauge glass $\nu \approx 1.13$.[25] z is more difficult to determine analytically, but for spin glasses, analytical and experimental results point to $z>4$. For a mean field superconductor, it is expected that $z \approx 2$.[33] Thus glasslike systems have both z and ν a factor of 2 greater than for ordered systems.

Based on I-V isotherm measurements on epitaxial YBCO at $1\times10^4 \le H \le 4\times10^4$ G, Koch *et al.*[10] found I-V scaling consistent with $\nu \approx 1.7$ and $z \approx 4.8$. They interpreted these values of ν and z as evidence for vortex glass superconductivity. For sintered YBCO at $H=5\times10^3$ and 1.5×10^4 G, Worthington *et al.* observed I-V scaling with $\nu=1.1\pm0.2$ and $z=4.6\pm0.2$.[8] They concluded that the similarity of their results with those of Koch *et al.* suggested that polycrystalline YBCO is also a vortex glass superconductor.

Our measurements at much smaller magnetic field values are consistent with $\nu \approx 1.3-1.6$ and $z \approx 2.6-3.4$. Thus our value for ν is similar to that reported for other systems and is consistent with that expected for an XY spin glass, although it is somewhat larger than predictions for a gauge glass.[25] z, on the other hand, is significantly lower than found in these other measurements. Since for spin glasses $z>4$, our result of $z \approx 3$ may be significant.

In addition to difficulties associated with various kinds of disorder in these materials, the interpretation of critical exponents in this system may be complicated by a feature unique to Josephson arrays. The changes that occur near T_c are due to the changes in Josephson coupling energy, whose average value increases from zero at T_{c0} to $\sim k_B T$ at T_c, just 1 K below T_{c0} at $H=0.5$ G. Thus in a Josephson array the phase transition is driven by large changes in coupling strength that occur over a relatively small temperature interval. This is different from a magnetic system, where the coupling strength is fixed and phase transitions are driven by changes in temperature. We are not aware of the effect that this difference is expected to have, if any, on the values of critical exponents.

CONCLUSION

We find that within the range of experimental I-V values accessible to us, the temperature-dependent evolution of I-V isotherms near the superconducting transition in these sintered YBCO superconductors is consistent with predictions of superconducting I-V scaling. Using the scaling form proposed by FFH, we extract from our I-V isotherm measurements a value for critical exponents $\nu \approx 1.3-1.6$ and $z \approx 2.6-3.4$. Our values for ν are in the general range of values reported from experiments on other YBCO superconducting systems. Our values for ν are similar to predictions for XY spin-glass systems, but are somewhat larger than predictions for an XY gauge glass. The values we obtain for z are significantly less than that expected for spin glasses, where $z>4$, and are significantly different than results obtained in other YBCO superconducting systems. As a result of the differences between our measurements and those obtained by Worthington *et al.*, and also based on our result of $z<4$, we believe that the origin of critical exponents and the significance of their values remains an open question in polycrystalline sintered YBCO.

ACKNOWLEDGMENTS

We gratefully acknowledge the assistance of B. M. Gong and J. C. W. Chien in fabricating our samples. This work was supported by Research Trust Funds administered by the University of Massachusetts at Amherst, by the polymer Materials Research Laboratory (NSF Grant No. DMR 90-23848), and by NSF Grant Nos. DMR 88-20517 and 91-22348.

[1] M. A. Dubson, S. T. Herbert, J. J. Calabrese, D. C. Harris, B. R. Patton, and J. C. Garland, Phys. Rev. Lett. **60**, 1061 (1988).
[2] I. Kasladenov, M. Mateev, I. V. Petrov. P. Vassilev, and J. Tikhov, Physica C **153-155**, 320 (1988).
[3] J. Evetts, B. A. Glowacki, P. L. Sampson, and M. G. Blamire, IEEE Trans. Magn. **25**, 2041 (1989).
[4] J. C. W. Chien, B. M. Gong, Y. S. Yang, J. M. Madsen, W. M. Tiernan, and R. B. Hallock, Physica C **165**, 279 (1990).
[5] W. M. Tiernan and R. B. Hallock, Phys. Rev. B **43**, 10 508 (1991).
[6] S. A. Sergeenkov, Physica C **167**, 339 (1990).
[7] J. C. Soret and L. Ammor, Physica C **177**, 45 (1991).
[8] T. K. Worthington, E. Olsson, C. S. Nichols, T. M. Shaw, and D. R. Clark, Phys. Rev. B **43**, 10 538 (1991).
[9] W. M. Tiernan and R. B. Hallock, Phys. Rev. B **46**, 3688 (1992).
[10] R. H. Koch, V. Foglietti, W. J. Gallagher, G. Koren, A. Gupta, and M. P. A. Fisher, Phys. Rev. Lett. **63**, 1511 (1989).
[11] W. M. Tiernan and R. B. Hallock (unpublished).
[12] W. M. Tiernan, Ph.D. dissertation, University of Massachusetts at Amherst, 1992 (unpublished).
[13] P. Chaudhari, R. H. Koch, R. B. Laibowitz, T. R. McGuire, and R. J. Gambino, Phys. Rev. Lett. **58**, 2684 (1987).
[14] J. F. Kwak, E. L. Venturni, P. J. Nigrey, and D. S. Ginley, Phys. Rev. B **37**, 9749 (1988).
[15] W. M. Tiernan and R. B. Hallock, Phys. Rev. B **43**, 10 508 (1991).
[16] D. Dimos, P. Chaudhari, and J. Mannhart, Phys. Rev. B **41**, 4038 (1990).

[17]D. S. Fisher, M. P. A. Fisher, and D. A. Huse, Phys. Rev. B **43**, 130 (1991).
[18]G. Deutscher, Y. Imry, and L. Gunther, Phys. Rev. B **10**, 4598 (1974).
[19]C. Ebner and D. Stroud, Phys. Rev. B **25**, 5711 (1982).
[20]C. Ebner and D. Stroud, Phys. Rev. B **28**, 5053 (1983).
[21]C. Ebner and D. Stroud, Phys. Rev. B **31**, 165 (1985).
[22]Y. Shih, C. Ebner, and D. Stroud, Phys. Rev. B **30**, 134 (1984).
[23]K. Binder and A. P. Young, Rev. Mod. Phys. **58**, 801 (1986).
[24]S. John and T. C. Lubensky, Phys. Rev. B **34**, 4815 (1986).
[25]A. Houghton and M. A. Moore, Phys. Rev. B **38**, 5045 (1988).
[26]J. Rosenblatt, in *Percolation, Localization, and Superconductivity,* edited by A. M. Goldman and S. A. Wolf (Plenum, New York, 1984), p. 431.
[27]C. Lebeau, J. Rosenblatt, A. Raboutou, and P. Peyral, Europhys. Lett. **1**, 313 (1986).
[28]A. Raboutou, J. Rosenblatt, and P. Peyral, Phys. Rev. Lett. **45**, 1035 (1980).
[29]M. S. Rzchowski, S. P. Benz, M. Tinkham, and C. J. Lobb, Phys. Rev. B **42**, 2041 (1990).
[30]S. P. Benz, M. S. Rzchowski, M. Tinkham, and C. J. Lobb, Phys. Rev. B **42**, 6165 (1990).
[31]D. C. Harris, S. T. Herbert, D. Stroud, and J. C. Garland, Phys. Rev. Lett. **67**, 3606 (1991).
[32]T. van Duzer, and C. W. Turner, *Principles of Superconducting Devices and Circuits* (Elsevier, New York, 1981).
[33]S.-K. Ma, *Modern Theory of Critical Phenomena* (Benjamin, London, 1976).
[34]M. P. A. Fisher, Phys. Rev. Lett. **62**, 1415 (1989).
[35]S. A. Wolf, D. U. Gubser, and Y. Imry, Phys. Rev. Lett. **42**, 324 (1979).
[36]A. F. Hebard and A. T. Fiory, Phys. Rev. Lett. **50**, 1603 (1983).
[37]P. C. Hohenberg and B. I. Halperin, Rev. Mod. Phys. **49**, 435 (1977).
[38]Refrigeration was provided by a CTI-Cryogenics model 22 closed-cycle refrigerator.
[39]J. W. Ekin, A. J. Panson, and B. A. Blankenship, Appl. Phys. Lett. **52**, 331 (1988).
[40]J. W. Ekin, T. M. Larson, N. F. Bergen, A. J. Nelson, A. B. Swartzlander, L. L. Kazmerski, A. J. Panson, and B. A. Blankenship, Appl. Phys. Lett. **52**, 1819 (1988).
[41]J. C. W. Chien, B. M. Gong, J. M. Madsen, and R. B. Hallock, Phys. Rev. B **38**, 853 (1988).
[42]J. C. W. Chien, B. M. Gong, X. Mu, and Y. S. Yang, J. Polym. Sci. A **28**, 1999 (1990).
[43]R. Zallen, *The Physics of Amorphous Solids* (Wiley, New York, 1983).
[44]C. C. Tsueii, and T. K. Plasketh, Phys. Rev. B **36**, 833 (1987).
[45]M. Ausloos and C. Laurent, Phys. Rev. B **37**, 611 (1988).
[46]B. Oh, K. Char, A. D. Kent, M. Naito, M. R. Beasley, T. H. Geballe, R. H. Hammond, and A. Kapitulnik, Phys. Rev. B **37**, 7861 (1988).